

RESEARCH PAPER

Chemical Synthesis of Silver Nanoparticles as a Dynamic Oncoming Antiviral and Antibacterial Therapy

Wajeeh Kachi Obead ^{1*}, Rajaa Hendi. Salih ² and Aml Hendi Salih ¹

¹ Middle Technical University, Institute of Medical Technology, Al-Mansour, Iraq

² Department of Microbiology, College of Science, Mustansiriyah University, Iraq

ARTICLE INFO

Article History:

Received 14 August 2024

Accepted 20 December 2024

Published 01 January 2025

Keywords:

Cell line

Chemical reduction

Measles virus

Pathogenic bacteria

Silver nanoparticles

ABSTRACT

Silver nanoparticles (Ag NPs) are essential in treating viruses and bacteria, especially in light of antibiotic resistance. The research aims to manufacture them in a manner that enhances their therapeutic effect. The study utilised UV spectral analysis, zeta potential imaging, dynamics of light scattering (DLS), atomic forces microscopy (AFM), transmission electron microscopy (TEM), and flame-atomic absorption spectroscopy (FAAM) to analyse the stability, size and concentration of Ag NPs. The vaccine strain of measles virus (MeV) was cultivated in the Vero/hSLAM cell line, and the tissue culture infective dose 50% (TCID₅₀) was determined. We then tested the efficacy of various concentrations of Ag NPs in inhibiting the proliferation of different multiplicities of infection (MOIs) of the virus and as an antibacterial agent against specific antibiotic-resistant isolates via the well diffusion method. AgNPs exhibited a spherical morphology with an average diameter of 20 nm, a polydispersity index of 0.245±006 and a diameter variation of 23.06±0.6 nm. The concentration of Ag NPs was 176 µg/ml, and they effectively inhibited the growth of the MeV-inappropriate cell line at varying concentrations and MOIs. Gram-positive and Gram-negative pathogens were significantly affected by the application of Ag NPs. The measurement of the inhibition zone increased with the concentration of Ag NPs for all tested pathogenic bacteria. The biosynthesized Ag NPs possess the potential to serve as a suitable alternative to commercial antibiotics in controlling resistant bacteria and inhibiting viral infection.

How to cite this article

Obead W., Salih R. and Salih A. Chemical Synthesis of Silver Nanoparticles as a Dynamic Oncoming Antiviral and Antibacterial Therapy. J Nanostruct, 2025; 15(1):276-291. DOI: 10.22052/JNS.2025.01.027

INTRODUCTION

The persistent issue of chemotherapy is the ability of microorganisms and viruses to develop drug resistance [1]. Therefore, it requires the development of new drugs and therapeutic approaches. Nanotechnologies provide numerous opportunities for novel treatment strategies [2] and have recently garnered global attention as potential antimicrobial drugs. The significance of

nanotechnology arises from its ability to produce and employ materials with a nanoscale of 1-100 nm. This feature facilitates entry into many practical and applied fields, including science (energy and electronics), health, medicines, chemical applications, and various other fields. [3].

Silver nanoparticles (AgNPs) possess numerous physical and chemical properties, such as low toxicity, ease of preparation, ultra-small size,

* Corresponding Author Email: wjeeh.kachi@mtu.edu.iq



diverse synthesis methods and high capacity to interact with formulated treatments in host cells [4]. These unique characteristics and their broad-spectrum activity against bacteria, fungi, and viruses make AgNPs a promising antimicrobial agent [5]. AgNPs have been extensively examined in virology, bacteriology, and oncology, encouraging their application in medicine, their veridical properties have been reported against different viruses [6,7]. AgNPs have been extensively studied against clinical infections; they exhibit an excellent solubility profile, targeted distribution to the infection site, and sustained release with minimal side effects. On 22 February 2024, the World Health Organization (WHO) announced that more than half of the countries in the world anticipate critical measles outbreaks this year. The measles virus (MeV) is a member of the Morbillivirus genus related to the Paramyxoviridae family [8], causing highly acute febrile disease and possibly leading to death. Many programmes have been implemented to eradicate measles, but outbreaks of the virus persist in many countries. Antibiotic resistance is recognized in bacteriology as a critical public health concern worldwide.

The hazard of antimicrobial resistance has resulted from inappropriate use, misuse of marketable antibiotics and the lack of new antibiotics with novel mechanisms of action [9]. Moreover, the rapid proliferation of antibiotic resistance is due to the transfer of resistance genes from one bacterium to other bacterial species [10,11]. In this study, we tested the antiviral and antibacterial efficacy of AgNPs to inhibit certain bacterial isolates and the vaccinated strain of the MeV, thereby addressing the issue of microorganism resistance to antibiotics.

MATERIALS AND METHODS

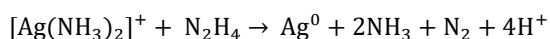
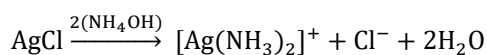
The study was conducted in the laboratories of the College of Science and the Iraqi Center of Cancer and Medical Genetics Research (ICCMGR), Mustansiriyah University, Iraq.

The chemicals employed in the experiment were silver chloride (AgCl), polyvinylpyrrolidone (PVP) with an average molecular weight of 40,000 and hydrazine hydrate (N₂H₄ 50%–60%) obtained from (Sigma-Aldrich) as well as ammonium hydroxide (NH₄OH 28%–30%) from BDH. The reagents were used in their pristine condition without any purification. The glassware was immersed in a solution of HNO₃ and H₂SO₄ at a molar ratio

of 1:3 for 30 min, subjected to sonication for 3 min, washed with double distilled water (DDW), dried in an oven for 1 h at 140 °C and exposed to a mixture of (95% H₂SO₄) and (30 wt.% of H₂O₂) in a 3:1 proportion for 30 min. subsequently, the glassware was subjected to a thorough cleaning process by immersed in DDW and sterilized in the oven at 100 °C for 1 h [12]. The whole procedure was iterated three times.

AgNPs synthesis (modified approach)

Silver chloride is a precursor for the synthesis of Ag NPs. Adding 71.66 mg of AgCl and 50 ml of ammonium hydroxide to the solution resulted in the complete dissolution of AgCl, yielding a clear solution devoid of solid particles. A specific quantity of polyvinyl pyrrolidone was included as a surfactant to stabilize the colloidal solution. The liquid was gently stirred to achieve a molar of Ag (NH₃)₂⁺: The PVP of 1:16, followed by the addition of 0.1 M hydrazine hydrate to the resultant solution. The solution was allowed to sit for 1 h via magnetic stirring at room temperature (RT). The equations below depict the successful generation of AgNPs through the reduction of [Ag (NH₃)₂]⁺ with hydrazine at RT [13,14].



Characterization

Analysis using Spectral Examination Techniques

The absorption spectrum of the AgNPs solution was analysed by ultraviolet–visible double optical spectrophotometry (UV-M90, BEL, Italy) at two separate time points: immediately after manufacture and 1 month later. The result aligned with the spectral characteristics of AgNPs nanoparticles in their aqueous solution.

Zeta Potential Evaluation

The SHIMADZU decomposer, designed for nano-sized zeta molecules, was used to examine colloidal AgNPs and assess their stability. The stability of the NPs was measured by measuring the surface charge density.

Characterization of AgNPs by atomic force microscopy (AFM)

The morphology, size and prevalence of the

synthesized AgNPs were determined by atomic force microscope (SHIMADZU, AA3000, JAPAN). To obtain images via AFM, we deposited a small volume of colloidal AgNPs solution on high-grade mica and allowed to dry at RT in a sterile laminar flow environment.

Analyzing AgNPs using Flame Atomic Absorption Spectrometry (FAAS)

The concentration of AgNPs was quantified using a Flame Atomic Absorption Spectrometer (FAAS) AA-7000 model by SHIMADZU, a renowned Japanese manufacturer. The measurement was conducted at a precise wavelength of 328.1 nm.

AgNPs were analysed using transmission electron microscopy (TEM)

The morphology and dimensions of AgNPs were determined via transmission electron microscopy (TEM) using a JEOL JEM-2100 microscope from Japan.

Analysis using Dynamic Light Scattering

The dimensions and distribution of particles in the colloids were quantified using a dynamic light scattering (DLS) instrument manufactured by Brookhaven Instruments (USA). The measurement conditions were as follows: a laser with a wavelength of 659 nm (He-Ne), a fixed scattering angle of 173°, a temperature of 25°C, a viscosity of 0.890 Cp and a medium refractive index of 1.330. The specimen was inserted into a quartz microcuvette, and measurements yielded the average result.

Cell line

The cell bank of the Iraqi Center for Cancer and Medical Genetics Research provided us with a VEROhSLAM cell line. These cells result from the transfection of Vero cells with pCXN2, a vector plasmid holding the gene of neomycin resistance, and an expression plasmid (pCAG-hSLAM), which encodes the receptor for the MeV [15].

Preservation of cell line

The cells were grown and maintained in minimum essential medium (MEM), supplemented with 10% fetal calf serum and an antibiotic / antimycotic Solution. When the cell density exceeded 80%, the growth medium was removed. Thereafter, 3 ml of trypsin- EDTA solution was added to T25 flasks, and after 1–2 min., the cells

detached, and 10% fetal calf serum (FCS)- MEM was introduced. The cells were redistributed at an appropriate concentration in the tissue culture flasks (sub-culture) and incubated at 37°C with 5% CO₂ [16].

Mesleas virus

This study utilised a vaccination strain of Live attenuated MeV (India). The virus propagated in VERO-hSLAM cells line using MEM; when the cytopathic effect (syncytia) exceeded 80%, the cells underwent three freeze–thaw cycles. The virus was aliquoted into sterile Eppendorf tubes and stored at –70°C.

Virus titration

The MeV tissue culture infected dose 50% (TCID₅₀) was used on the VERO-hSLAM cell line, with cell suspensions sub-cultured and inoculated in a 96-well microtitration plate containing 104 cells in 100 µL per well. After overnight cultivation, cell growth reached 80%, and the medium was removed to prepare a serial tenfold dilution of MeV (10⁻¹– 10⁻⁹), which was allocated to the wells (50 µL/well) at a ratio of 4 wells per dilution. Meanwhile, the maintenance medium (200 µL) was injected into each control well, and the plate was incubated for 1 h at 37°C to facilitate viral adsorption. Subsequently, maintenance media with 3%–5% FCS was added (200 µL/each well) after washing the cells with PBS to eliminate the non-associated virus. The plate was analysed for 5-6 days, and TCID₅₀ was determined using the equation of Reed and Muench [17].

Cytotoxicity of MeV

The VERO-hSLAM cell line was cultured in a 96-well micro-titer plate (1 x 10⁴ cells/well). Cells were exposed to the virus via discarded medium. The cells were exposed to multiplicities of infections (MOI) with MeV at 1, 3, 6 and 10 by adding 50 µL of each viral MOI; three replicates were used for each MOI, whereas control cells remained untreated. The plate was incubated at 37°C for 1 h, with shaking every 10 min to facilitate the distribution and attachment of the virus to the cells. Subsequently, the cells were rinsed with PBS, and 0.1 mL of maintenance medium containing 5% FCS was added. After 72 h, the cells were rinsed with PBS, and 5 µg/mL MTT solution was introduced for a duration of up to 2 h. After discarding the supernatant and drying the cells,

100 μL of DMSO was added to each well. The extinction values at 570 nm were determined photometrically via spectrophotometric analysis [18].

Antiviral effect of AgNPs

The AgNPs were evaluated for antiviral activity. Cells were seeded onto 96-well plates at a density of 1×10^4 cells per well and incubated for 24 h at 37 °C. Cells monolayer were incubated with different MOIs (1, 3, 6 and 10) of MeV (three wells for each MOI) for 1 h to facilitate viral adsorption. The virus was removed, and various concentrations of AgNPs (100, 50, 25 and 12.5) were introduced, which were dissolved in MEM-free serum. For the positive control, cells were infected with the same concentrations of the virus but without AgNPs. The negative control consisted only of MEM supplemented with 5% FBS. On the third day after infection, MTT assay was performed in brief, the medium was discarded, and cells in each well were incubated with 50 μL of MTT solution (5 mg/mL) for 2 h. at 37°C. MTT solution was discarded, and 100 μL dimethyl sulfoxide (DMSO) was added to dissolve the insoluble formazan crystal. Optical density was measured at a wavelength of 492 nm with an ELISA reader.

Pathogenic isolates

Sixteen pathogenic isolates, four from each bacterial species, were obtained from different clinical samples. They were *Staphylococcus aureus*, *Staphylococcus epidermidis*, *Pseudomonas aerogenosa*, and *Escherichia coli*. The isolates were obtained from wound infections that exhibited antibiotic resistance. The identification of isolates was conducted using Gram staining, biochemical tests and a VITEK-2 compact system.

AgNPs antibacterial activity

The antimicrobial efficacy was tested against each bacterial isolate, adjusted to 0.6 OD and uniformly applied onto Mueller–Hinton agar plate by using sterile cotton pads. Five wells, each 6 mm in diameter, were stamped with sterilized micropipette tips on the prepared plates, into which synthesized AgNPs were introduced at with varying concentrations of 100, 50, 25, and 12.5 μL (15 μL in each well); sterilized physiological saline served as the control well [19]. The plates were incubated at 37°C for 24 h, and the width of the inhibition zones was recorded in millimeters (mm)

using an antibiotic zone scale referenced in [20]. All the trials were conducted in triplicate.

Statistical Analysis

The research findings were subjected to statistical analysis using the Statistical Package for Social Science (SPSS) version 26 to determine the significance of variation. Statistical significance was defined as $p \leq 0.05$ for significant or $p \leq 0.0$ for highly significant. All statistically assessed samples were run in triplicate, unless stated otherwise. Data were expressed as mean \pm standard deviation and approved using Graph Pad Prism version 8 (Graph Pad Software Inc.). To analyse the efficacy of the antiviral, we used CompuSyn software (ComboSyn Inc., Paramus, USA) to compute the Chou-Talalay antagonism indices (CIs) and variable ratios of MeV and chemotherapeutics. Additionally, we employed alternative precise formulae to obtain the CIs. A confidence interval (CI) ranging from 0.9 to 1.1 indicates additivity. A CI of 0.9 indicates synergism, whereas a CI of 1.1 indicates antagonism.

RESULTS AND DISCUSSION

Size distribution of NPs studied using UV/Vis spectroscopy

The synthesis of AgNPs included the reaction between silver ions as oxidizing factors and hydrazine hydrate as reducing agents. AgNPs were synthesized by reacting silver ions as oxidising agents with hydrazine hydrate as reducing agents. The first observed occurrence was a color change. The solution underwent a colour change from a light-yellow hue to a reddish-brown shade toward the conclusion of the reaction (Fig. 1a). The UV-Vis spectra of colloidal AgNPs (Fig. 1b) exhibited a distinct surface plasmon resonance (SPR) band at 423 nm. This peak confirmed the creation of AgNPs [21]. To evaluate the stability of colloidal AgNPs, we immediately recorded the spectra after production and again following 1 month without stirring or ultrasonication. Fig. 1a demonstrates no significant alterations in the location or form of the SPR band. However, we found a modest modification in the absorption intensities of the colloidal AgNPs, which shifted from 223 nm to 228 nm. Furthermore, the artificially produced AgNPs were stable at RT, with no clumping observed over 1 month. Our findings were aligned with the results reported in the reference [22].

Zeta potential of AgNPs

Fig. 2 displays the zeta potential values of colloidal AgNPs. The surface charge was +45.89 mV. Significant values were achieved, indicating exceptional durability. Therefore, this silver liquid was ready for use.

AFM Analysis

The primary data were extracted from AFM images of the shape and size of the NPs [23]. Figs.

3 and 4 show the AFM images and size distribution histogram of AgNPs, respectively. The particles exhibited a spherical morphology with an average diameter of 20.56 nm, which was consistent with previously reported values [24].

Concentration of colloidal AgNPs in the stock solution

Before measuring their concentration, the AgNPs were sterilised using a Millipore with

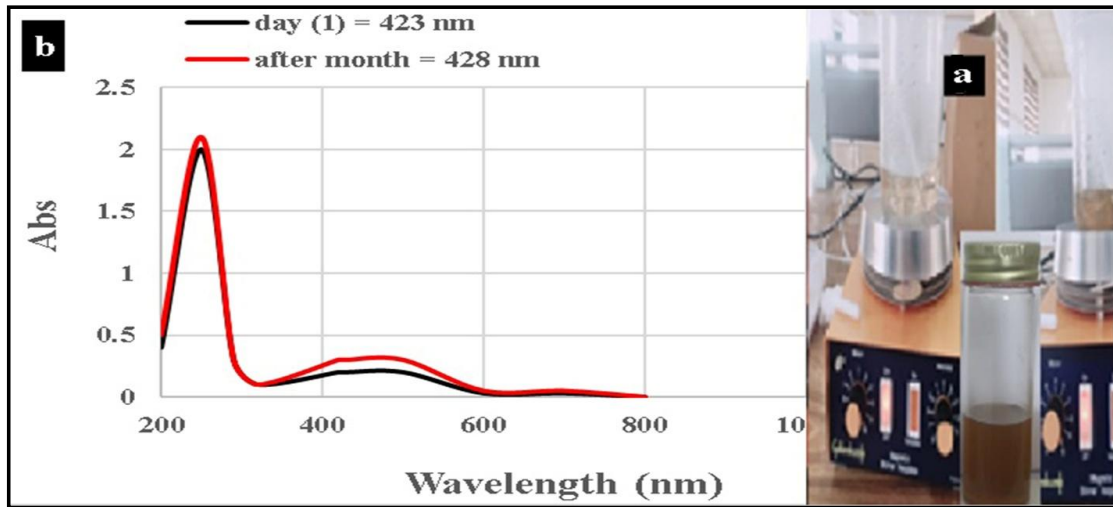


Fig. 1. (a) Phases of color transition in the production process (b) The UV-Vis spectrum of silver nanoparticles (AgNPs) was synthesized directly after the cessation of the response using the reduction process. Furthermore, following one month of storage at ambient temperature.

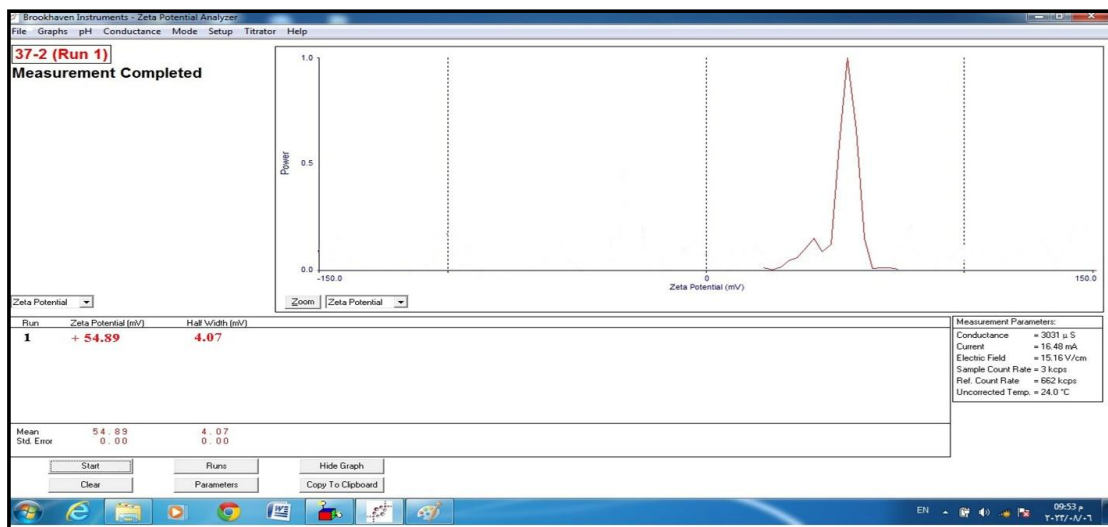


Fig. 2. Analyzed the zeta potential of silver nanoparticles (AgNPs) synthesized by the chemical reduction process.

a diameter of 0.45 μm . The concentration of silver ions was determined using a flame atomic absorption instrument, employing the standard curve methodology shown in Fig. 5. The result yielded a concentration of around 100 $\mu\text{g}/\text{mL}$.

Analysis of AgNPs via TEM

Fig. 6 displays the TEM images of Ag NPs. It was also used to determine the mean dimensions of AgNPs. The TEM observations were obtained at a

distance of about 20 nm.

Analysis of AgNPs via DLS

The DLS study yielded the polydisperse system, which offered the particles' half-width, diameters, and size. The results demonstrated remarkable monodispersity, as illustrated in Fig. 7, revealing an effective hydrodynamic diameter of 23.06 ± 0.6 nm and a polydispersity of 0.245 ± 0.06 nm for the synthesized AgNPs.

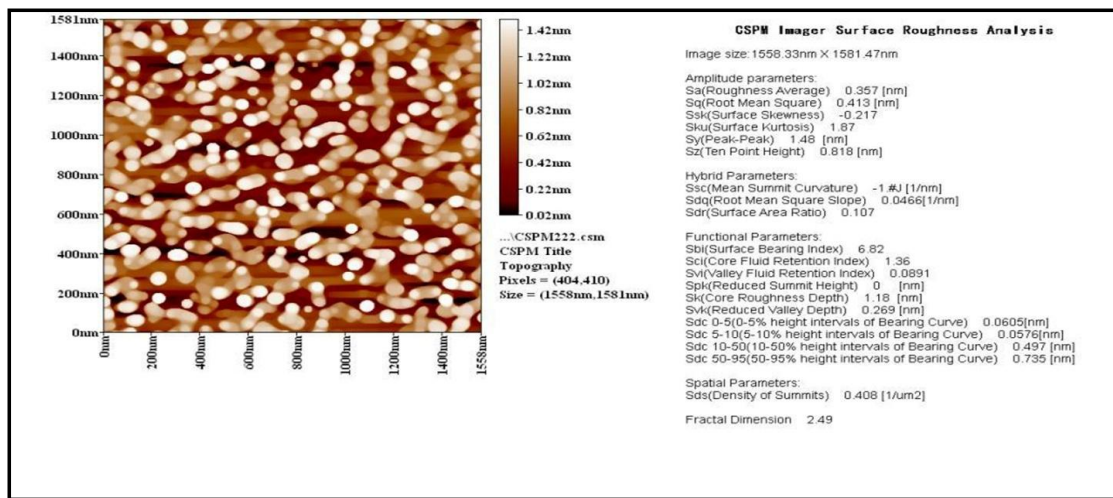


Fig. 3. Images obtained using Atomic Force Microscopy showing silver nanoparticles.

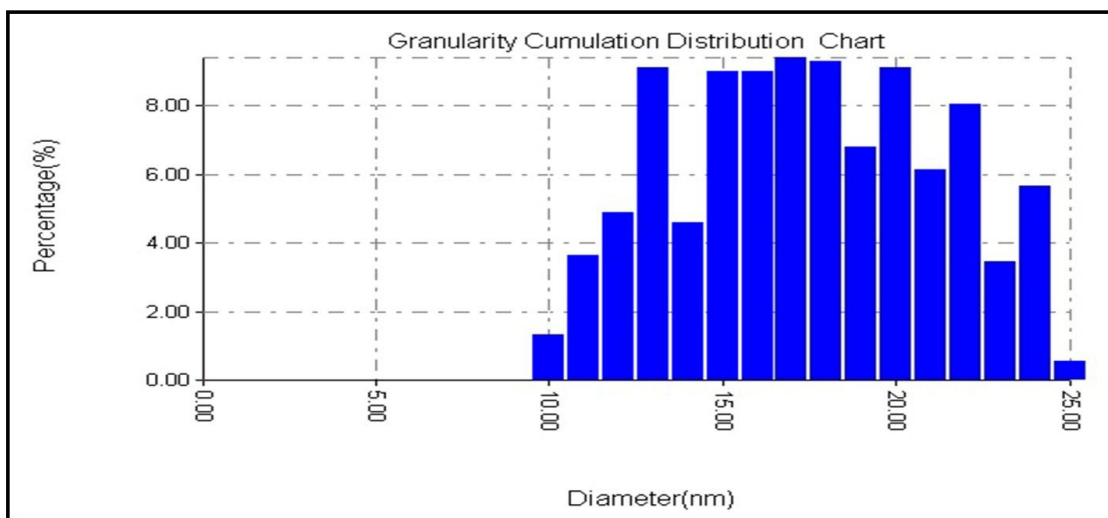


Fig. 4. AFM images were used to generate a histogram showing the size distribution of silver nanoparticles.

*Using produced AgNPs as an antiviral tool
Virus titration (tissue culture infective dose 50%)*

Vero/hSLAM cells were used to determine the TCID50 of MeV. This method involves infecting cultured cells with the tenfold dilution of the virus and observing the cytopathic effect in the cells, this effect is characterized by round cells, aggregations, small vacuoles in the cytoplasm of the infected cells and formation of syncytia (large multinucleated cells), resulting from the fusion

of infected cells, which produce plaques. The endpoint at 50% was $2 \times 10^{6.5}$ TCID50 / 100 MI.

Cytotoxic effect of MeV

The hallmark of MeV infection in Vero/hSLAM cells was the development of syncytia. This phenomenon was a characteristic cytopathic effect caused by this virus. It led to tissue damage and a viral transmission mechanism compared with the control, which showed no pathological

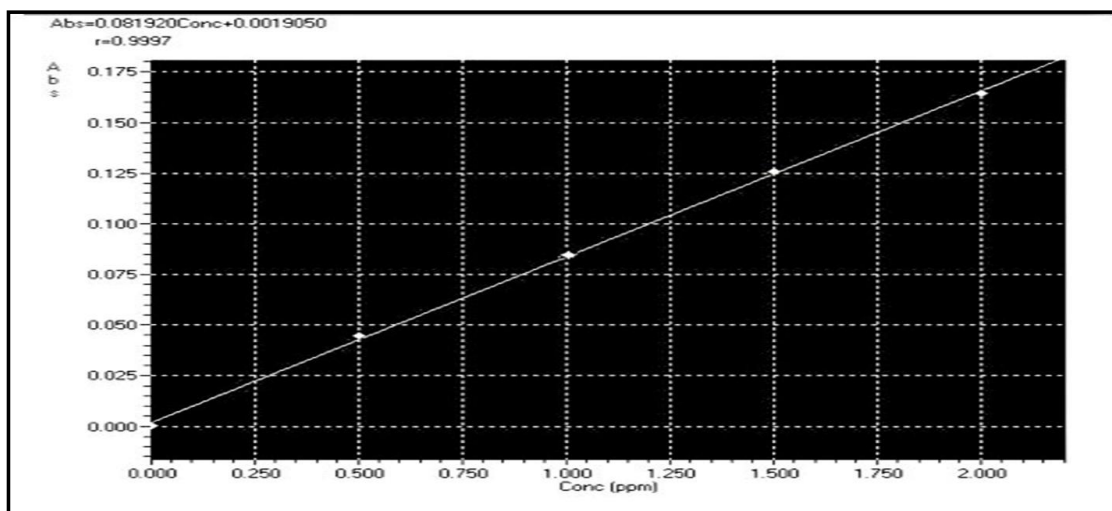


Fig. 5. Quantification of silver ions using flame atomic absorption spectroscopy using a standard curve.

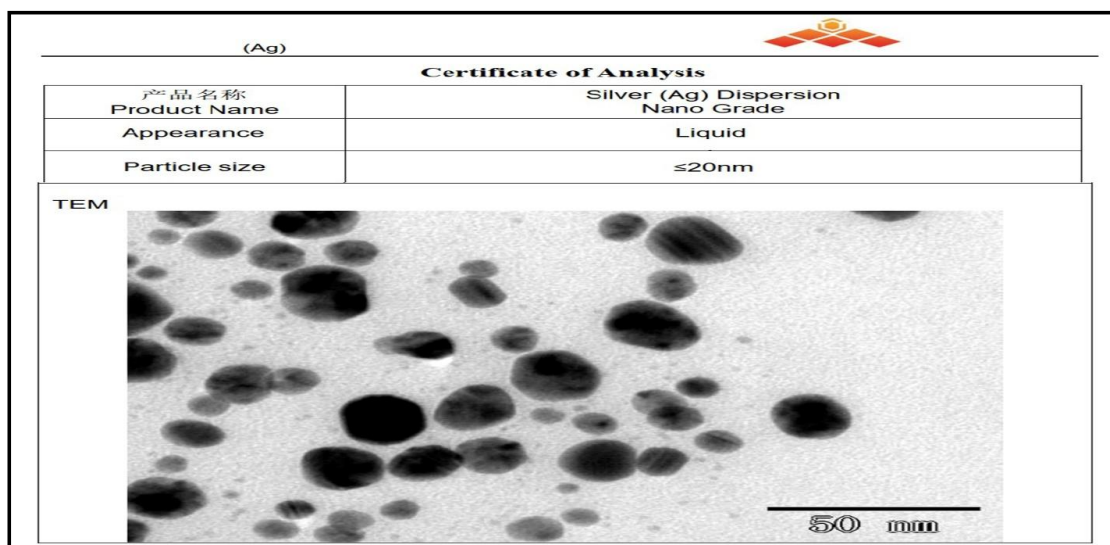


Fig. 6. TEM images for Ag NPs.

changes.

The results in Fig. 8 showed that the most significant cellular damage occurred at MOI of 10 after 72 h of infection with inhibition percentage of 93.29 ± 1.73 . The cell mortality rate declined when the MOI decreased (88.83 ± 1.52 , 60.99 ± 0.72 and 57.86 ± 1.36 for MOIs of 6, 3 and 1, respectively). We found significant differences among the four virus concentrations ($p=0.02$).

Antiviral activity of AgNPs

The Vero/hSLAM cell line facilitated the

proliferation of MeV within 24 h, with the cytopathic effects manifesting as rounding of infected cells and the formation of small, numerous cytoplasmic vacuoles, which became noticeable with time until 72 h of infection. The exposure of cells infected with different MOIs of the MeV to various concentrations of AgNPs resulted in the inhibition of the pathogenic effect of the virus on the cells. The inhibition percentages declined to 82.71 ± 1.52 , 80 and 82 ± 1.53 in the first two concentrations used (MOI=10+100 $\mu\text{g}/\text{mL}$ and MOI=6+50 $\mu\text{g}/\text{mL}$). However, when the

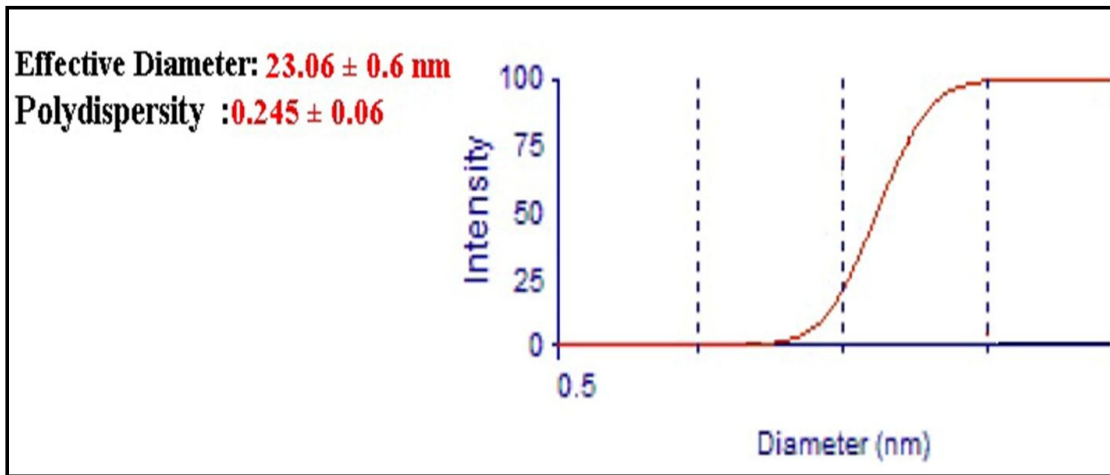


Fig. 7. DLS approach evaluation of silver nanoparticles' distribution of size.

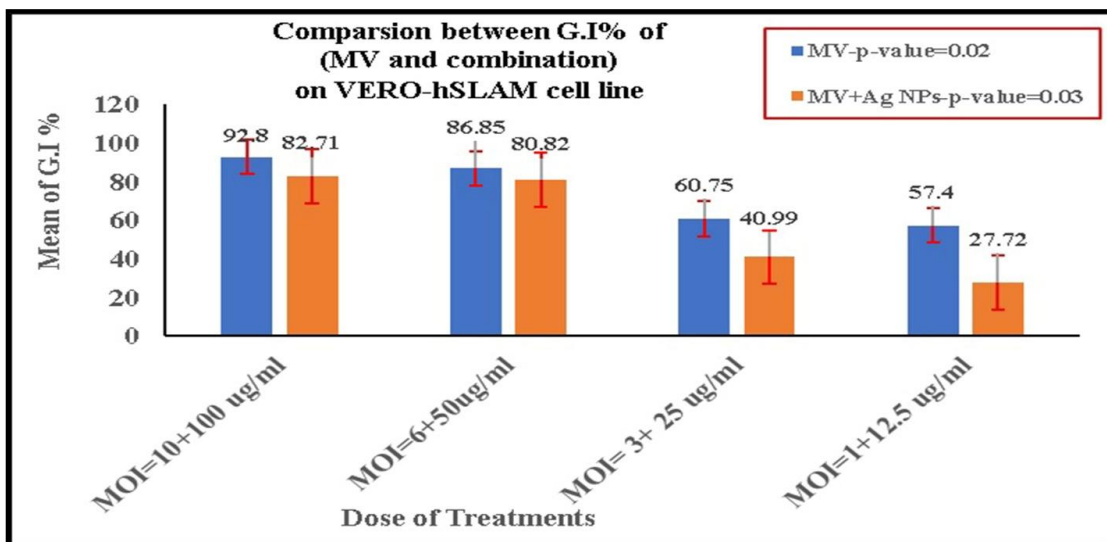


Fig. 8. Comparison between three treatments (MV alone and MV+ Ag NPs) at all points on the VERO-hSLAM cell line.

MOI of the virus declined, the effect of Ag NPs decreased (40.99 ± 1.52 and 27.72 ± 1.52) for the combination (MOI= 3+ 25 $\mu\text{g}/\text{mL}$ and MOI=1+12. $\mu\text{g}/\text{mL}$) as shown in Table 1 and Fig. 8.

In addition, Table 2 and Fig. 9 show that AgNPs exerted an antagonism effect with MeV in the Vero/hSLAM cell line after 72 h of exposure period at all concentrations used in this study

Antibacterial Inhibitory Activity of AgNPs In-vitro

The formulated AgNPs efficiently inhibited the growth of Gram-positive and Gram-negative pathogens. The maximum growth inhibition zones (mean \pm SD = 18.7 ± 0.2 mm) were observed at 100 μg of AgNPs against *P. aerogenosa*, thereafter decreasing to 16.6 ± 0.7 , 15.9 ± 0.1 and 13.9 ± 0.4 for concentrations of 50, 25 and 12.5 $\mu\text{g}/\text{mL}$,

Table 1. The cytotoxic effect of MV and combination (MV + AgNPs) on VERO-hSLAM cell line.

Treatments	G.I% of MV Mean \pm SD	G.I% of combination (MV + AgNPs) Mean \pm SD
MOI=10+100 $\mu\text{g}/\text{ml}$	93.29 ± 1.73	82.71 ± 1.52
MOI=6+50 $\mu\text{g}/\text{ml}$	88.83 ± 1.52	80.82 ± 1.53
MOI= 3+ 25 $\mu\text{g}/\text{ml}$	60.99 ± 0.72	40.99 ± 1.52
	p-value <0.05* significance ; P-value <0.01** Highly significance	
P-value =	0.02*	0.03*

Table 2. the antagonism effect of MV and AgNPs on the VERO-hSLAM cell line.

Point	MV(MOI)	Ag NPs ($\mu\text{g}/\text{ml}$)	G.I%	CI	Effect
1	10	100	0.82	3.49873	Antagonism
2	6	50	0.801	2.20957	Antagonism
3	3	25	0.403	5.55445	Antagonism
4	1	12.5	0.279	3.39694	Antagonism

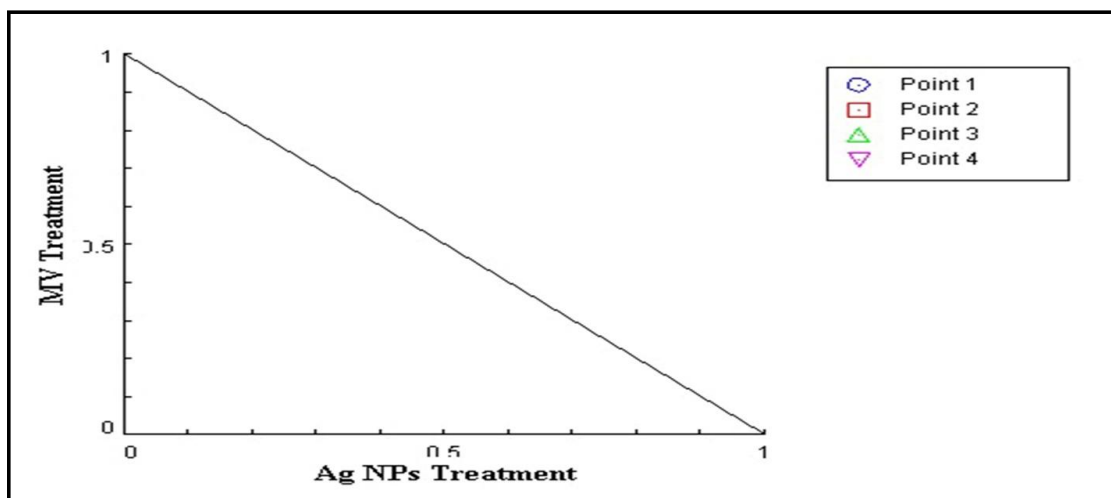


Fig. 9. Isobologram analysis showing the antagonism effect between MV and AgNPs on VERO-hSLAM cell line.

respectively. A highly significant difference was found among the effect of the four dilutions ($P \leq 0.0002$). The strains of *E. coli* resulted in less inhibition (Mean \pm SD = 16.6 ± 0.4 , 15.9 ± 0.6 , 15 ± 0.5 , 13 ± 0.1) at the same concentrations with high significant difference ($P \leq 0.0001$) as shown in Table 3.

When comparing the effect of Ag NPs on negative bacteria, we found that *P. aeruginosa* was affected more than *E. coli*, especially in the two highest concentrations of 100 and 50 $\mu\text{g/mL}$, as shown in Fig. 10 and Table 4.

The results in Fig. 11 and Table 5 showed a highly significant inhibition effect for Ag NPs ($P \leq$

0.009 and 0.007) on the growth of the *S. aureus* and *S. epidermidis* strains, respectively, at the four dilutions.

Against *S. aureus*, the maximum growth inhibition zones (mean \pm SD = 17.2 ± 0.52 mm) were found at a concentration of 100 μg of Ag NPs, then decreased to (Mean \pm SD = 16.4 ± 0.51 , 14 ± 0.2 , 12.8 ± 0.73) for concentrations of (50, 25, 12.5, respectively).

Whereas the minimal zone of growth inhibition by Ag NPs (Mean \pm SD = 12.2 ± 0.6 mm) was found at 12.5 $\mu\text{g/mL}$ against *S. epidermidis*, followed by 13.6 ± 0.7 , 15.5 ± 0.1 and 16.5 ± 0.3 .

The results indicate that the inhibition zone

Table 3. Mean \pm SD inhibitory effect of different concentrations of silver nanoparticles against the four bacterial isolates types as anti-bacterial agent.

Bacterial isolates	Conc. 100 ($\mu\text{g/ml}$)	Mean \pm SD	Conc. 50 ($\mu\text{g/ml}$)	Mean \pm SD	Conc. 25 ($\mu\text{g/ml}$)	Mean \pm SD	Conc. 12.5 ($\mu\text{g/ml}$)	Mean \pm SD	P-value
staphylococcus aureus	17.50		16.55		14.00		13.00		0.009*
staphylococcus aureus	17.00	17.2 ± 0.52	16.00	16.4 ± 0.51	14.2	14 ± 0.2	12.00	12.8 ± 0.73	*
staphylococcus aureus	17.80		17.00		13.8		13.1		
staphylococcus aureus	16.8		16.3		14.00		13.4		
staphylococcus epidermidis	16.20		15.7		14.1		12.5		
staphylococcus epidermidis	16.75	16.5 ± 0.3	15.5	15.5 ± 0.1	14.4	13.6 ± 0.70	12.00	12.2 ± 0.6	0.007*
staphylococcus epidermidis	16.20		15.7		13.00		11.8		
staphylococcus epidermidis	16.70		15.5		13.5		13.00		
pseudomonas aeruginosa	18.30		17.00		16.3		14.00		
pseudomonas aeruginosa	19.00	18.7 ± 0.2	17.2	16.6 ± 0.7	15.8	15.9 ± 0.1	14.3	13.9 ± 0.4	0.0002
pseudomonas aeruginosa	18.5		15.8		16.00		13.5		
pseudomonas aeruginosa	18.7		16.8		16.00		14.1		
E. coli	17.00		16.0		14.8		12.8		
E. coli	17.30	16.6 ± 0.4	16.0	15.9 ± 0.6	15.00	15 ± 0.5	13.00	13 ± 0.1	0.0001
E. coli	16.5		15.2		14.5		13.2		
E. coli	16.00		16.5		15.6		13.00		

$P > 0.05$ N.S (N.S = No Significance), $P \leq 0.05$ S, (S = Significance)*, $P \leq 0.01$ H.S (H.S = Highly Significance)**

Table 4. Mean \pm SD effect of different conc. of Ag NPs against *P. aeruginosa* and *E. coli*.

Conc of AgNPs ($\mu\text{g/ml}$)	Zone of G.I (mm) of <i>P. aeruginosa</i> Mean \pm SD	Zone of G. I (mm) of <i>E. coli</i> Mean \pm SD
100	18.7 ± 0.2	16.6 ± 0.4
50	16.6 ± 0.7	15.9 ± 0.6
25	15.9 ± 0.1	15 ± 0.5
12.5	13.9 ± 0.4	12.3 ± 0.1
<i>P-value</i> =	0.0002**	0.0001**

p-value <0.05* significance
; P-value <0.01** Highly significance

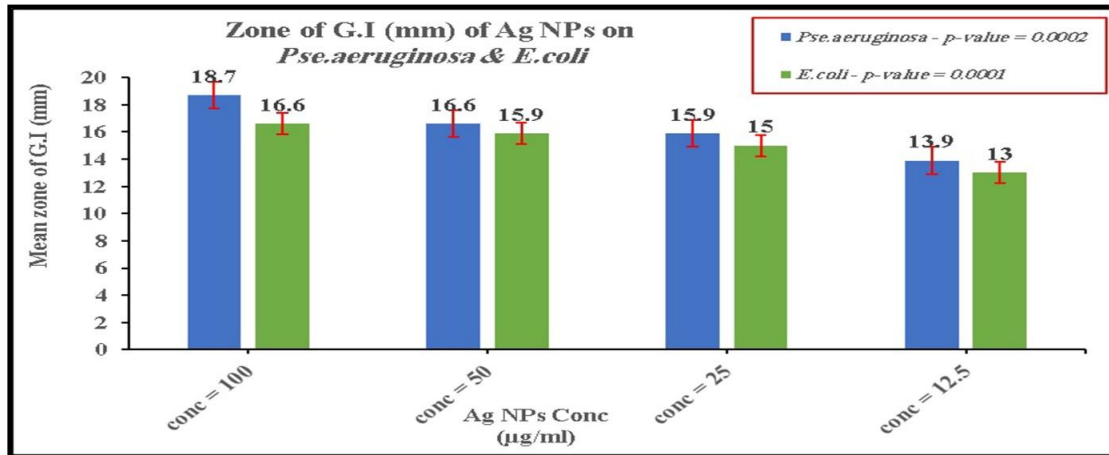


Fig. 10. mean zone of inhibition presented by *P. aeruginosa* and *E. coli* treated with different concentrations of Ag NPs.

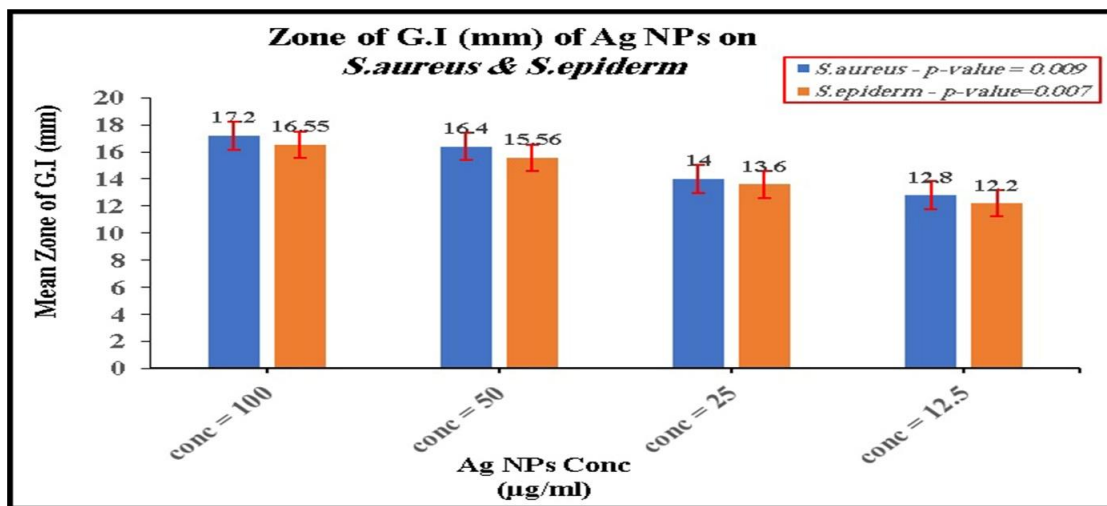


Fig. 11. Mean zone of inhibition presented by *S. aureus* and *S. epidermidis* treated with different concentrations of AgNPs.

Table 5. Mean ± SD effect of different conc. of Ag NPs against *S. aureus* and *S. epiderm*.

Conc of AgNPs (µg/ml)	Zone of G.I (mm) of	
	<i>S. aureus</i> Mean ± SD	<i>S. epiderm</i> Mean ± SD
100	17.2 ± 0.52	16.5 ± 0.3
50	16.4 ± 0.51	15.5 ± 0.1
25	14 ± 0.2	13.6 ± 0.7
12.5	12.8 ± 0.73	12.2 ± 0.6
<i>P-value</i> =	0.009**	0.007**

p-value <0.05* significance
; P-value <0.01** Highly significance

increased with the concentration of AgNPs, and AgNPs exhibited antimicrobial activity, even at low concentrations. However, the effect was more pronounced in Gram-negative strains than in Gram-positive strains as show in Fig. 12

The incidence of infections caused by antibiotic-resistant bacteria is rising worldwide; such infections exacerbate patient disease and mortality and pose economic challenges for the health system. Nanotechnology has introduce promising agents for combating viruses and bacteria, mainly silver nanoparticles AgNPs [25].

However, Ag NPs are widely used as they are inexpensive and have definite antibacterial activity, limited resistance progress, negligible immunological response and cytotoxicity [26-29].

The features of AgNPs render them suitable for use in medical and healthcare products for the treatment or prevention of infections [30,31]. The optimal mechanism of interaction that makes AgNPs highly effective remains unclear due to the different conflicting processes influencing their activity [31].

UV/Vis spectroscopy analysis revealed that AgNPs produced UV-visible spectra via

the phenomenon known as surface plasmon resonance (SPR), resulting from the interaction among light, electromagnetic radiation and free electrons, The presence of AgNPs was verified by detecting a peak at 423 nm and a colour transition from yellow to yellowish brown. The colour shift was most evident within the wavelength range of 350-450 nm, corresponding to the SPR of AgNPs [32]. Furthermore, the stability of colloidal AgNPs was assessed by UV/vis spectroscopy by examining the convergence of the peak in the UV spectrum, which shifted slightly from 423 nm immediately after production to 428 nm after 1 month. This phenomenon validated the stability of the colloidal solution. The results of the zeta analysis confirmed the stability of the manufactured colloidal AgNPs. This test quantified the surface charge, providing accurate insights into the properties of the majority of the molecules in the suspension. As a result of electrostatic repulsion, the stability of the dispersion improves when the zeta value exceeded +30 or -30 mV. The zeta potential +54.89 mV indicated that the manufactured particles were stable in the liquid [33].

To determine the shape and size of the

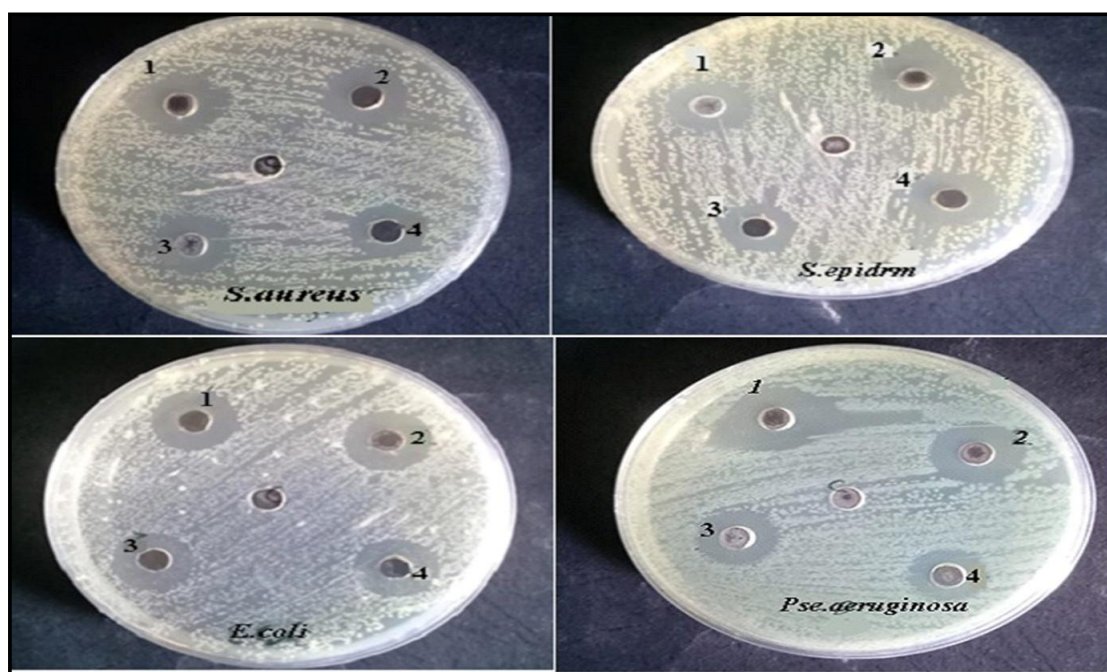


Fig. 12. Antibacterial effect of AgNPs against different bacterial isolates with various concentration (100,50,25,12.5) as 1,2,3,4 respectively.

nanoparticles (morphology), we used AFM through a direct surface image of the sample. The prepared AgNPs exhibited a spherical morphology, systematically positioned on the silicon surface, with an average size of 20 nm. This result was consistent with the findings from TEM and DLS analysis [34].

TEM operates by depositing a droplet of AgNPs solution onto a conventional 200-mesh grid to obtain information regarding the shape and size. The AgNPs exhibited a spherical morphology, with an average diameter of 20 nm or less. This analysis provided an extensive understanding of the dimensions and dispersion patterns of the NPs. The findings were consistent with the outcomes of AFM and aligned with the results of prior research [35]. The size disparity and stability of AgNPs are crucial for their utilization in medical and other fields. Confirmation was achieved by DLS, which provides significant and beneficial details. The analysis revealed an average particle size distribution of 23.06 ± 0.6 nm, which closely corresponded to the measurements obtained from AFM and TEM. In this examination, the size distribution was determined by analysing the Brownian motion of the suspended NPs. This motion, referred to as the diffusion coefficient, is related to the speed and is quantified by the polydispersion index (PDI). The PDI is between 0 and 1, with values close to zero indicating a narrower size distribution. A value of 0 implies a high level of homogeneity; conversely, a value close to 1 indicates the opposite. In this case, the result of 0.245 ± 0.06 nm suggested that the suspension was homogenous and stable. This finding was in agreement with the results of the zeta test. In the current study, the NPs were tested on an MeV isolate. This study concluded that the Vero/hSLAM cell line supported a measles-attenuated viral strain with a high inhibition percentage after 72 h of infection compared with the typical morphology of the cell control [36]. Cytotoxicity was assessed through (A) modification of normal cell morphology and (B) cell culture viability via MTT assay. The cultured cells were checked daily for signs of cytopathic effect. The results of our research highlighted that AgNPs demonstrated good antiviral activity against MeV in its suitable cells; several studies have revealed that AgNPs primarily act by physically interacting with the free or bound viral particle. Thus, AgNPs can function as virucidal agents [37]. The volume and size of

the AgNPs influenced the antiviral action of the complex system, which improved with increased concentration and reduced sizes of AgNPs. Antimicrobial substitutes such as NPs are favorable for treating bacterial infections, mainly due to the emerging risk of antibiotic resistance [38]. Li, Y. et al. Revealed that varying incubation times of AgNPs with the virus allowed for the observation of viral morphology by TEM. Their findings demonstrated that AgNPs can directly interact with the virus and damage the viral morphology [39]. A recent study described the antimicrobial potential of PLAL-AgNPs created by an inventive physical method named PLAL. The new PLAL-AgNPs showed no toxic properties on the classically used cells. Antiviral activity was assessed against the enclosed HSV-1 and the non-enclosed PV-1. The PLAL-AgNPs inhibited viral units during the early stage of viral infection [40,41]. The results proved that AgNPs exhibited remarkable antimicrobial activity against pathogenic bacterial strains, even at low concentrations. Different concentrations of AgNPs inhibited all bacterial species, and the inhibition zone was amplified with an increase in the concentration of NPs, consistent with previous studies [42,43]. The development of microbial resistance to NPs is limited by different mechanisms of action of AgNPs, which influence various aspects of bacterial growth and metabolism [43]. The possibility of AgNPs as antibiotics is linked to their numerous mechanisms of action, which attack microorganisms in multiple structures at a time, enabling them to kill diverse bacterial species [44]. The critical property of an antibacterial agent is its capability to interact with and alter the bacterial outer membrane, facilitating internalization [45]. In addition to its ability to disrupt and penetrate the cell membrane by modifying its structure and permeability, leading to rupture and loss of the cytoplasmic content, it can similarly enter the cell and modify DNA and protein structures and functions through interaction with phosphorus or sulfur groups. AgNPs may adjust the respiratory chain in the inner membrane by interaction with thiol groups in the enzymes; inhibiting adenosine triphosphate production; generating free radicals and reactive oxygen species; causing damage to intracellular structures; leading to the oxidation of proteins, lipids and DNA breaks; and triggering the apoptosis pathway. Ag NPs disrupt cell division, leading to cell death [46-48]. The release of positively charged ions upon

suspension, their oxidation dissolution abilities and the ability to replace ligands facilitate their binding to the negatively electric bacterial cell wall, thereby enhancing their bactericidal efficacy [49]. Tang, S. et al. demonstrated that Ag NPs have broad antibacterial activity against *E. coli* and *S. aureus*. Given their diminutive size, Ag NPs rapidly penetrate cell membranes and disrupt intracellular processes [50]. Hasan, K. M. F. et al and Trzcińska-Wencel, J. et al. reported that the most dominant mechanism in Gram-negative bacteria may involve pit formation and membrane disruption. By contrast, in Gram-positive bacteria, the most dominant mechanism may be the damage of the thick peptidoglycan layer, and Gram-positive bacteria are less sensitive to the action of AgNPs than Gram-negative bacteria [51,52].

Although the cell wall of *E. coli* is more damaging than that of *S. aureus*, which could appeal to AgNPs with increased intensity, this fact might not produce a significant influence as Gram-negative and positive bacteria possess negatively charged cell wall, and membrane disruption produced by metal NPs is more injurious for Gram-negative bacteria than for Gram-positive bacteria [53].

Similarly, Nath H. et al. reported that *P. aeruginosa* is sensitive to AgNPs [54]. Yuan, Y.-G. et al. found that AgNPs caused decreased lactate dehydrogenase (LDH) activity and decreased adenosine triphosphate levels in *P. aeruginosa* and *S. aureus* [55], Li, W.-R. et al. proved that the AgNPs inhibits the respiratory chain dehydrogenase by converting various enzymes, such as glycerol-3-phosphate dehydrogenase, into dihydroxyacetone in *S. aureus*, thereby interfering with the metabolism and growth of the bacteria cells. TEM images have illustrated that AgNPs affect the integrity of the *E. coli* membrane by depolarization and destabilization [56]. Vazquez-Muñoz, R. et al. discovered that oxidative stress of AgNPs causes alteration in kynurenine protein and activation of kynurenine pathways, thereby inhibiting the bacterial growth of *P. aerogenosa*, *E. coli* and *S. aureus* [46].

CONCLUSION

In conclusion, this research demonstrated that AgNPs successfully targeted the MeV vaccine strain and exerted a remarkable effect on pathogenic strains. Additional experiments may elucidate viral mortality pathways and parameters activated by this approach to support its antiviral

and antibacterial properties.

ACKNOWLEDGMENT

We are thankful to Mustansiriyah University, Iraqi Center for Cancer and Medical Genetic Research and Department of Chemistry (IBS/UPM) for their technical assistance.

CONFLICT OF INTEREST

The authors declare that there is no conflict of interests regarding the publication of this manuscript.

REFERENCES

1. Lauring AS, Frydman J, Andino R. The role of mutational robustness in RNA virus evolution. *Nature reviews Microbiology*. 2013;11(5):327-336.
2. Lysenko V, Lozovski V, Lokshyn M, Gomeniuk YV, Dorovskih A, Rusinchuk N, et al. Nanoparticles as antiviral agents against adenoviruses. *Advances in Natural Sciences: Nanoscience and Nanotechnology*. 2018;9(2):025021.
3. Taha TB, Barzinjy AA, Hussain FHS, Nurtayeva T. *Nanotechnology and Computer Science: Trends and advances*. *Memories - Materials, Devices, Circuits and Systems*. 2022;2:100011.
4. Ghosh U, Sayef Ahammed K, Mishra S, Bhaumik A. The Emerging Roles of Silver Nanoparticles to Target Viral Life Cycle and Detect Viral Pathogens. *Chem Asian J*. 2022;17(5):e202101149-e202101149.
5. Tariq M, Mohammad KN, Ahmed B, Siddiqui MA, Lee J. Biological Synthesis of Silver Nanoparticles and Prospects in Plant Disease Management. *Molecules (Basel, Switzerland)*. 2022;27(15):4754.
6. Lee N-Y, Ko W-C, Hsueh P-R. Nanoparticles in the Treatment of Infections Caused by Multidrug-Resistant Organisms. *Front Pharmacol*. 2019;10:1153-1153.
7. Mba IE, Nweze EI. Nanoparticles as therapeutic options for treating multidrug-resistant bacteria: research progress, challenges, and prospects. *World J Microbiol Biotechnol*. 2021;37(6):108-108.
8. Hübschen JM, Gouandjika-Vasilache I, Dina J. Measles. *The Lancet*. 2022;399(10325):678-690.
9. Szul M. Causes Behind the Global Crisis of Increasing Antibiotic Resistance and Strategies to stop this. *Polygence*; 2024.
10. Lerminiaux NA, Cameron ADS. Horizontal transfer of antibiotic resistance genes in clinical environments. *Can J Microbiol*. 2019;65(1):34-44.
11. Sun D, Jeannot K, Xiao Y, Knapp CW. Editorial: Horizontal Gene Transfer Mediated Bacterial Antibiotic Resistance. *Front Microbiol*. 2019;10:1933-1933.
12. Gargioni C, Borzenkov M, D'Alfonso L, Sperandeo P, Polissi A, Cucca L, et al. Self-Assembled Monolayers of Copper Sulfide Nanoparticles on Glass as Antibacterial Coatings. *Nanomaterials (Basel, Switzerland)*. 2020;10(2):352.
13. Slepíčka P, Slepíčková Kasálková N, Siegel J, Kolská Z, Švorčík V. Methods of Gold and Silver Nanoparticles Preparation. *Materials (Basel, Switzerland)*. 2019;13(1):1.
14. Ajaypraveenkumar A, Henry J, Mohanraj K, Sivakumar G, Umamaheswari S. Characterisation, Luminescence and Antibacterial Properties of Stable AgNPs Synthesised from AgCl by Precipitation Method. *Journal of Materials Science*

- and Technology. 2015;31(11):1125-1132.
15. Yanagi Y, Ono N, Tatsuo H, Hashimoto K, Minagawa H. Measles Virus Receptor SLAM (CD150). *Virology*. 2002;299(2):155-161.
 16. Freshney RI. *Culture of Animal Cells*: Wiley; 2010 2010/09/20.
 17. Reed LJ, Muench H. A Simple Method of Estimating Fifty Per Cent Endpoints. *Am J Epidemiol*. 1938;27(3):493-497.
 18. Wang F. *Culture of Animal Cells: A Manual of Basic Technique, Fifth Edition*. In *Vitro Cellular and Developmental Biology - Animal*. 2006;42(5):169.
 19. Zafar S, Zafar A. Biosynthesis and Characterization of Silver Nanoparticles Using Phoenix dactylifera Fruits Extract and their In Vitro Antimicrobial and Cytotoxic Effects. *The Open Biotechnology Journal*. 2019;13(1):37-46.
 20. Balouiri M, Sadiki M, Ibensouda SK. Methods for in vitro evaluating antimicrobial activity: A review. *Journal of pharmaceutical analysis*. 2016;6(2):71-79.
 21. Le NTT, Nguyen DH, Nguyen NH, Ching YC, Pham Nguyen DY, Ngo CQ, et al. Silver Nanoparticles Ecofriendly Synthesized by *Achyranthes aspera* and *Scoparia dulcis* Leaf Broth as an Effective Fungicide. *Applied Sciences*. 2020;10(7):2505.
 22. Mollick MMR, Bhowmick B, Maity D, Mondal D, Roy I, Sarkar J, et al. Green synthesis of silver nanoparticles-based nanofluids and investigation of their antimicrobial activities. *Microfluid Nanofluid*. 2013;16(3):541-551.
 23. Mustafa G, Islam MU, Zhang W, Arshad MI, Jamil Y, Anwar H, et al. Investigation of the Role of Ce³⁺ Substituted Ions on Dielectric Properties of Co-Cr Ferrites Prepared by Coprecipitation Method. *J Electron Mater*. 2016;45(11):5830-5838.
 24. Mohaghegh S, Osouli-Bostanabad K, Nazemiyeh H, Javadzadeh Y, Parvizpur A, Barzegar-Jalali M, et al. A comparative study of eco-friendly silver nanoparticles synthesis using *Prunus domestica* plum extract and sodium citrate as reducing agents. *Adv Powder Technol*. 2020;31(3):1169-1180.
 25. Jorge de Souza TA, Rosa Souza LR, Franchi LP. Silver nanoparticles: An integrated view of green synthesis methods, transformation in the environment, and toxicity. *Ecotoxicology and Environmental Safety*. 2019;171:691-700.
 26. Yaqoob AA, Umar K, Ibrahim MNM. Silver nanoparticles: various methods of synthesis, size affecting factors and their potential applications—a review. *Applied Nanoscience*. 2020;10(5):1369-1378.
 27. Yin IX, Zhang J, Zhao IS, Mei ML, Li Q, Chu CH. The Antibacterial Mechanism of Silver Nanoparticles and Its Application in Dentistry. *International journal of nanomedicine*. 2020;15:2555-2562.
 28. Nguyen NPU, Dang NT, Doan L, Nguyen TTH. Synthesis of Silver Nanoparticles: From Conventional to 'Modern' Methods—A Review. *Processes*. 2023;11(9):2617.
 29. Bruna T, Maldonado-Bravo F, Jara P, Caro N. Silver Nanoparticles and Their Antibacterial Applications. *Int J Mol Sci*. 2021;22(13):7202.
 30. Rezk N, Abdelsattar AS, Makky S, Hussein AH, Kamel AG, El-Shibiny A. New formula of the green synthesised Au@Ag core@shell nanoparticles using propolis extract presented high antibacterial and anticancer activity. *AMB Express*. 2022;12(1):108-108.
 31. Dingli D, Cascino MD, Josić K, Russell SJ, Bajzer Ž. Mathematical modeling of cancer radiotherapy. *Math Biosci*. 2006;199(1):55-78.
 32. Abdussalam-Mohammed W, Mohamed L, Abraheem MS, Mansour MMA, Sherif AM. Biofabrication of Silver Nanoparticles Using Teucrium Apollinis Extract: Characterization, Stability, and Their Antibacterial Activities. *Chemistry (Easton)*. 2023;5(1):54-64.
 33. Mohd Yasin SM, Badruddin IA, Johan MR. Super Stability of Ag Nanoparticle in Crystalline Lamellar (Lc) Liquid Crystal Matrix at Different pH Environment. *Symmetry*. 2019;12(1):31.
 34. Kazemi M, Akbari A, Sabouri Z, Soleimanpour S, Zarrinfar H, Khatami M, et al. Green synthesis of colloidal selenium nanoparticles in starch solutions and investigation of their photocatalytic, antimicrobial, and cytotoxicity effects. *Bioprocess and Biosystems Engineering*. 2021;44(6):1215-1225.
 35. Jayakar V, Lokapur V, Nityasree BR, Chalannavar RK, Lasrado LD, Shantaram M. Optimization and green synthesis of zinc oxide nanoparticle using *Garcinia cambogia* leaf and evaluation of their antioxidant and anticancer property in kidney cancer (A498) cell lines. *Biomedicine*. 2021;41(2):206-222.
 36. Al-Khedhairi AA, Wahab R. Silver Nanoparticles: An Instantaneous Solution for Anticancer Activity against Human Liver (HepG2) and Breast (MCF-7) Cancer Cells. *Metals*. 2022;12(1):148.
 37. Luceri A, Francese R, Lembo D, Ferraris M, Balagna C. Silver Nanoparticles: Review of Antiviral Properties, Mechanism of Action and Applications. *Microorganisms*. 2023;11(3):629.
 38. Mori Y, Ono T, Miyahira Y, Nguyen VQ, Matsui T, Ishihara M. Antiviral activity of silver nanoparticle/chitosan composites against H1N1 influenza A virus. *Nanoscale research letters*. 2013;8(1):93-93.
 39. Li Y, Lin Z, Zhao M, Xu T, Wang C, Hua L, et al. Silver Nanoparticle Based Codelivery of Oseltamivir to Inhibit the Activity of the H1N1 Influenza Virus through ROS-Mediated Signaling Pathways. *ACS Applied Materials and Interfaces*. 2016;8(37):24385-24393.
 40. Morone MV, Chianese A, Dell'Annunziata F, Folliero V, Lamparelli EP, Della Porta G, et al. Ligand-Free Silver Nanoparticles: An Innovative Strategy against Viruses and Bacteria. *Microorganisms*. 2024;12(4):820.
 41. Salleh A, Naomi R, Utami ND, Mohammad AW, Mahmoudi E, Mustafa N, et al. The Potential of Silver Nanoparticles for Antiviral and Antibacterial Applications: A Mechanism of Action. *Nanomaterials (Basel, Switzerland)*. 2020;10(8):1566.
 42. Akshaya T, Aravind M, Manoj Kumar S, Divya B. Evaluation Of In-Vitro Antibacterial Activity Against Gram-Negative Bacteria Using Silver Nanoparticles Synthesized from *Dyopsis Lutescens* Leaf Extract. *Journal of the Chilean Chemical Society*. 2022;67(2):5477-5483.
 43. Wang J, Shu K, Zhang L, Si Y. Effects of Silver Nanoparticles on Soil Microbial Communities and Bacterial Nitrification in Suburban Vegetable Soils. *Pedosphere*. 2017;27(3):482-490.
 44. Raut S, Bhatavadekar A, Chougule R, Lekhak U. Silver nanoparticles synthesis from *Crinum moorei*: Optimization, characterization, kinetics and catalytic application. *S Afr J Bot*. 2024;165:494-504.
 45. Menichetti A, Mavridi-Printezi A, Mordini D, Montalti M. Effect of Size, Shape and Surface Functionalization on the Antibacterial Activity of Silver Nanoparticles. *Journal of functional biomaterials*. 2023;14(5):244.
 46. Vazquez-Muñoz R, Meza-Villezas A, Fournier PGJ, Soria-Castro E, Juarez-Moreno K, Gallego-Hernández AL, et al. Enhancement of antibiotics antimicrobial activity due to

- the silver nanoparticles impact on the cell membrane. *PLoS One*. 2019;14(11):e0224904-e0224904.
47. de Lacerda Coriolano D, de Souza JB, Bueno EV, Medeiros SMdFRDS, Cavalcanti IDL, Cavalcanti IMF. Antibacterial and antibiofilm potential of silver nanoparticles against antibiotic-sensitive and multidrug-resistant *Pseudomonas aeruginosa* strains. *Brazilian journal of microbiology : [publication of the Brazilian Society for Microbiology]*. 2021;52(1):267-278.
 48. Herbin HB, Aravind M, Amalanathan M, Mary MSM, Lenin MM, Parvathiraja C, et al. Synthesis of Silver Nanoparticles Using *Syzygium malaccense* Fruit Extract and Evaluation of Their Catalytic Activity and Antibacterial Properties. *Journal of Inorganic and Organometallic Polymers and Materials*. 2022;32(3):1103-1115.
 49. Godoy-Gallardo M, Eckhard U, Delgado LM, de Roo Puente YJD, Hoyos-Nogués M, Gil FJ, et al. Antibacterial approaches in tissue engineering using metal ions and nanoparticles: From mechanisms to applications. *Bioactive materials*. 2021;6(12):4470-4490.
 50. Tang S, Zheng J. Antibacterial Activity of Silver Nanoparticles: Structural Effects. *Advanced Healthcare Materials*. 2018;7(13).
 51. Hasan KMF, Xiaoyi L, Shaoqin Z, Horváth PG, Bak M, Bejő L, et al. Functional silver nanoparticles synthesis from sustainable point of view: 2000 to 2023 – A review on game changing materials. *Heliyon*. 2022;8(12):e12322-e12322.
 52. Trzcińska-Wencel J, Wypij M, Rai M, Golińska P. Biogenic nanosilver bearing antimicrobial and antibiofilm activities and its potential for application in agriculture and industry. *Front Microbiol*. 2023;14:1125685-1125685.
 53. Varghese M, Balachandran M. Antibacterial efficiency of carbon dots against Gram-positive and Gram-negative bacteria: A review. *Journal of Environmental Chemical Engineering*. 2021;9(6):106821.
 54. Nath H, Khataniar A, Bania KK, Mukerjee N, Al-Hussain SA, Zaki MEA, et al. Nano-functionalization and evaluation of antimicrobial activity of *Tinospora cordifolia* against the TolB protein of *Pseudomonas aeruginosa* - An antibacterial and computational study. *Front Microbiol*. 2023;14:1138106-1138106.
 55. Yuan Y-G, Peng Q-L, Gurunathan S. Effects of Silver Nanoparticles on Multiple Drug-Resistant Strains of *Staphylococcus aureus* and *Pseudomonas aeruginosa* from Mastitis-Infected Goats: An Alternative Approach for Antimicrobial Therapy. *Int J Mol Sci*. 2017;18(3):569.
 56. Li W-R, Xie X-B, Shi Q-S, Zeng H-Y, Ou-Yang Y-S, Chen Y-B. Antibacterial activity and mechanism of silver nanoparticles on *Escherichia coli*. *Applied Microbiology and Biotechnology*. 2009;85(4):1115-1122.